Toward Plug and Play Myoelectric Control via One-Shot Latent Representation Alignment

Zubaidah Al-Mashhadani, *Graduate Student Member, IEEE*, Trevor Overton, *Student Member, IEEE*, Di Wu, *Member, IEEE*, and Mohsen Rakhshan, *Member, IEEE*

***Abstract*— Myoelectric control has emerged as a common tool for human-machine interaction with applications in prostheses, rehabilitation, and mixed reality. Despite the growing research and promising results in controlled laboratory settings, there are challenges to its widespread adoption. During activities of daily living, factors such as limb position, electrode shift, cross-day variability, and individual differences reduce the reliability of controllers. Moreover, most existing work to address these issues is validated on individuals without limb differences, limiting clinical generalizability. We posit that even in the presence of these confounding factors, the intention of performing a specific gesture remains similar. Hence, a common underlying dynamics of muscle activity could be leveraged to create a robust myoelectric controller. Therefore, we propose a one-shot learning framework based on Multi-set Canonical Correlation Analysis to align the latent representation of the surface electromyography signals to achieve reliable myoelectric control across limb positions, days, and individuals with only minimal calibration data from a new condition (i.e., limb position, day, or individual). Importantly, we show that our framework generalizes from individuals without limb differences to an individual with a congenital limb difference despite different muscular physiology. Therefore, our framework can eliminate the need for retraining and data-hungry models, promoting plug-and-play myoelectric control robust to variations in limb position, day, and individual.**

***Index Terms*— Electromyography, myoelectric control, pattern recognition, machine learning, human–machine interaction.**

Received 14 May 2025; revised 18 September 2025; accepted 23 October 2025. Date of publication 27 October 2025; date of current version 6 November 2025. *(Corresponding author: Mohsen Rakhshan.)*

This work involved human subjects or animals in its research. Approval of all ethical and experimental procedures and protocols was granted by the University of Central Florida's Institutional Review Board under Application No. 3/22/2024.

Zubaidah Al-Mashhadani and Di Wu are with the Department of Electrical and Computer Engineering, College of Engineering, University of Central Florida, Orlando, FL 32816 USA (e-mail: zubaidah.almashhadani@ucf.edu; di.wu@ucf.edu).

Trevor Overton is with the Department of Electrical and Computer Engineering, the College of Engineering, and the Burnett School of Biomedical Sciences, University of Central Florida, Orlando, FL 32816 USA (e-mail: trevor.overton@ucf.edu).

Mohsen Rakhshan is with the Disability, Aging and Technology, the Faculty Cluster Initiative, and the Department of Electrical and Computer Engineering, College of Engineering, University of Central Florida, Orlando, FL 32816 USA (e-mail: mohsen.rakhshan@ucf.edu).

Digital Object Identifier 10.1109/TNSRE.2025.3626255

I. Introduction

With the advancement of wearable technologies, prosthetics, and mixed-reality environments, there is an increasing demand for intuitive and natural human-machine interaction (HMI) paradigms. Myoelectric control, which translates electromyography (EMG) signals into actionable commands, has extended beyond clinical prosthetics to broader HMI applications, including robot control [1], [2], [3], game interaction [4], rehabilitation [5], and mixed reality [6].

Surface EMG (sEMG) signals are commonly used to decode movement intent and are considered well-suited for myoelectric applications due to their non-invasive nature, compact form factor, ability to capture subtle muscular activity, and low power consumption [7], [8]. However, sEMG signals are inherently variable and sensitive to external and physiological factors such as perspiration, limb position, electrode displacement, muscle fatigue, and individual anatomical and behavioral differences [9], [10], [11], [12], [13]. Moreover, prior studies demonstrated that even intramuscular EMG signals are susceptible to such variability [14]. These variabilities due to the confounding factors introduce distributional shifts in the EMG feature space, which degrade decoding reliability and deteriorate generalization across limb positions, recording days, and individuals. Consequently, despite promising research results, real-world deployment of EMG-based control systems remains limited without effective strategies to mitigate non-stationarity. Changes in limb position and posture influence muscle shape and length, thereby affecting sEMG signals and degrading decoding performance [9]. Moreover, muscle activation patterns vary with the orientation of adjacent joints in addition to the primary joints involved. Together, these variations define the limb position effect, further compounding the complexity of a robust myoelectric decoding [6], [15], [16], [17]. Temporal factors further exacerbate the variability in EMG signals. More specifically, muscle contractions exhibit strong temporal dependencies, with activation patterns influenced by prior states and evolving dynamically over time [18]. Several strategies have been proposed to mitigate the effects of limb position variability on myoelectric decoding accuracy. For instance, Jiang et al. [6] developed an unsupervised, self-calibrating random forest model adapted to varying arm positions. Furthermore, Cheng et al. [19] proposed a

position-independent canonical correlation analysis (CCA)-based framework for classifying 13 hand gestures across three limb positions, achieving an accuracy of 76.11% overall.

Temporal or cross-day variability adds an additional layer of complexity. Changes in electrode placement, skin impedance, or neuromuscular adaptation over time alter the distribution of sEMG features [20]. These disparities in feature space between training and new recording sessions degrade generalization and often necessitate frequent model retraining [21], [22], [23]. Recent efforts have aimed to improve the robustness of myoelectric controllers across multiple days. Jiang et al. [24] investigated cross-day stability by evaluating 55 temporal–spectral–spatial features and optimizing a Support Vector Machine (SVM) model, achieving 88.75% accuracy of 28 hand gestures. Botros et al. [21] and Jiang et al. [25] further addressed cross-day variability through feature optimization and channel interpolation techniques, achieving decoding accuracies of 95.7% and 91.9%, respectively. Shi et al. [26] evaluated eight unsupervised transfer learning algorithms based on CNNs, and achieved a cross-day average accuracy of 87.94% using CORrelation Alignment (CORAL). Domenico et al. [27] investigated non-stationarities in myocontrol over multiple days using incremental learning to mitigate distribution shifts. Similarly, Jiang et al. [28] achieved long-term robustness with a pretrained self-calibrating random forest model that adapts to a new user with a single trial per gesture and maintains accuracy gains over time.

Finally, individual differences introduce a significant distribution shift, driven by muscle anatomy, subcutaneous fat distribution, movement strategies, and contraction force levels [20], [29]. Prior studies have shown that variations in force levels during gesture execution also impact the model performance [18]. As a result, pre-trained models often fail to generalize effectively to new users without extensive calibration or model retraining. However, large-scale datasets such as EMG-EPN612 [30] have enabled zero-shot learning frameworks for intersubject generalization [31]. Yet, these approaches often rely on computationally intensive models ill-suited for real-time applications [32], [33], [34]. Zheng et al. [35] proposed an alternative approach by employing an adaptive K-nearest neighbor (KNN) algorithm for user adaptation, reporting average recognition accuracies of 83.05% across 4 hand gestures using double Myo armbands [36].

Alternative methods such as CCA have shown promise in biomedical signal processing for identifying shared representations with low computational cost [12], [13], [19], [37]. CCA, first introduced by Hotelling in 1936 [38], is a statistical method for identifying correlations between two multivariate datasets. Xue et al. [12] designed a user-independent myoelectric controller using CCA and domain adaptation, achieving an average cross-subject classification accuracy of 78.15% on 13 hand gestures. Donati et al. [23] addressed cross-day variability in sEMG by applying CCA to map new-day recordings into the feature space of a reference session. While effective for improving classifier stability across days, this method is restricted to pairwise alignment and does not account for limb position effect or cross-subject differences.

In practice, most CCA-based myoelectric controllers rely on aligning only two datasets at a time, often designating one as an "expert". This pairwise alignment strategy overlooks the broader shared latent dynamics that may exist across multiple datasets, limiting the ability to uncover a global structure necessary for robust generalization. Although several extensions of CCA have been proposed to support alignment across multiple datasets [39], [40], [41], [42], [43], a unified framework that can address variability due to limb position, day-to-day differences, and individual users simultaneously remains underexplored.

Additionally, generalizing models to individuals with upper limb difference (ULD) is particularly challenging due to different neuromuscular organization [44]. Nevertheless, most existing work is validated on individuals without ULD (non-ULD), leaving a gap in clinical translation.

To bridge these gaps, we employ Multi-set Canonical Correlation Analysis (MCCA) [42] to jointly align sEMG signals across positions, days, and individuals (including an individual with ULD). By extracting a shared latent representation from multiple datasets, our approach generalizes more effectively across diverse acquisition scenarios, while requiring minimal calibration. More specifically, we introduce a one-shot calibration strategy that maps new recordings into the training feature space, eliminating the need for model retraining while reducing the effect of limb position, cross-day variability, and cross-user variability on the accuracy of the controller. This approach can be a significant step towards a plug-and-play controller for HMI paradigms.

II. Methods

We designed a series of controlled experiments to examine the performance of our myoelectric control across conditions with variabilities due to limb positions, acquisition days, and individuals, including upper-limb differences. Our approach leveraged MCCA [42] to extract shared latent representations and obtain high classification accuracy with minimal calibration or re-training of the controller.

A. Participants and Data Acquisition Setup

The dataset was collected from 18 non-ULD subjects and one ULD subject (ages 18–36; 15 males, 4 females) across five days. The study was approved by the University of Central Florida's Institutional Review Board (study 6576; Approved: 3/22/2024). All subjects provided informed consent before taking part in the experiment.

We conducted the experiments using our developed open-source system, the Common Arm Position Signal Acquisition System (CAPSAS) [45], [46]. CAPSAS consists of 16 LED-animated hexagons that provide real-time visual cues to guide subjects. Each hexagon is equipped with an infrared (IR) proximity sensor that detects when the subject's hand reaches the designated position. CAPSAS was used to label limb positions and to implement an automated experimental control. The automated control of trial initiation and progression in CAPSAS eliminated experimenter interference and enabled consistent, high-throughput data acquisition.

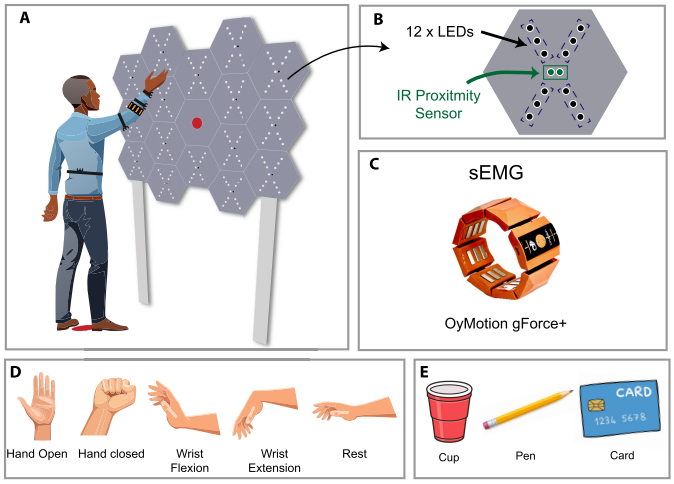

Fig. 1. Experimental setup and task design. (A, B, C) CAPSAS data acquisition system: the setup included 16 hexagonal modules, each equipped with 12 LEDs for visual cueing and an infrared (IR) proximity sensor for trial triggering and timestamping. Muscle activity was recorded using an 8-channel OYMotion gForce+ armband. (D, E) Task protocol: subjects performed five hand gestures: hand open, hand closed, wrist extension, wrist flexion, and rest; object-grasping tasks were executed using 3D-printed objects: pencil, card, and cup. The experiment consisted of five sessions across three task modes: two static, two dynamic, and one object-grasp session. In static mode, gestures were held at a specific position for five seconds. In dynamic and object-grasp sessions, tasks followed a structured sequence: (3s hold → 3s move → 3s hold). All tasks were cued automatically using CAPSAS LED animations.

Each subject performed the experiments standing at a standardized reference position in front of the CAPSAS system, based on their anthropometric measurements. The device height was adjusted so that the arm was raised to 90°, the hand aligned with the center of the device (red button in Figure 1) to reach the most proximal targets without stepping forward.

Trials were self-initiated, and subjects could proceed at their own pace without a fixed inter-trial interval. A 5-minute break was given after a fixed number of trials (depending on the mode of the experiment; see below) to prevent fatigue. sEMG signals were recorded using an 8-channel OYMotion gForcePro+ armband (12-bit resolution) positioned approximately 4 cm below the elbow on the dominant arm for non-ULD subjects, and on the residual forearm distal to the elbow for the ULD subject. We maintained consistency of the armband orientation across the subjects by aligning its on/off button oriented laterally when the participant was in the anatomical position. A 3D-printed extension socket was fabricated based on a personalized 3D scan and measurements for the ULD subject. When attached to the residual limb, the socket simulated the weight loading and inertial properties associated with operating a prosthetic hand. Data were acquired at a sampling rate of *500 Hz* and synchronized using Lab Streaming Layer (LSL) [47].

Each non-ULD subject performed all three experimental modes (i.e., static, dynamic, object; see below), whereas the ULD subject completed static and dynamic modes.

Static mode: Non-ULD subjects performed one of five hand gestures (hand open, hand closed, wrist flexion, wrist extension, and rest), whereas the ULD subject performed three gestures (hand open, hand close, rest) (Figure 1). Each gesture was held for 5 seconds at a position indicated by CAPSAS and performed three times per arm position, resulting in 240 randomized trials per session for non-ULD subjects and 144 trials for the ULD subject. There were two sessions of static mode across two different days.

Dynamic mode: Subjects executed the same hand gestures as in static mode while transitioning between positions. The start and end positions were instructed automatically by CAPSAS. Each trial was structured as follows: 3 seconds hold at the start position → 3 seconds movement → 3 seconds hold at the end position. For timekeeping, CAPSAS changed the LEDs' color to indicate the remaining time during the 3-second movements. The subjects were familiarized with the task and the meanings of the LED colors in a practice session prior to the experiment. Each session included 180 trials for non-ULD subjects and 108 for the ULD subject, comprising 12 ordered transitions among four possible positions, with each transition repeated three times per gesture. Similar to static mode, there were two sessions of dynamic mode across two different days.

Object mode: Due to the modular design of the CAPSAS, we could study the grasp and movement of real-life objects. We used three 3D printed objects: pen, card, and cup. Similar to the dynamic mode, the start and end positions for each object grasp were instructed automatically by CAPSAS. Each trial was also similar to the dynamic mode, but with grasping objects. That is, the subject grasped the object and held it at the starting position for 3 seconds → 3 seconds movement → 3 seconds hold at the end position, and replaced the object at that position. Each session included 216 trials, consisting of 12 ordered transitions among four possible positions, with each transition repeated six times for each object. There was only one session of the object mode.

B. EMG Signal Processing and Feature Engineering

Raw sEMG signals were recorded using the Oymotion gForce+ armband, which includes an onboard hardware bandpass filter ($20 - 500Hz$). Recordings were segmented into individual trials based on the IR sensor time stamps. For each session, the segmented sEMG data were structured according to the experiment mode: static ($240 \times 2500 \times 8$), dynamic ($180 \times 4500 \times 8$), and object grasp ($216 \times 4500 \times 8$), where each matrix follows the format (*trials* $\times$*time samples*$\times$ *channels*). In dynamic sessions, only the 3-second movement period was retained, resulting in a reduced matrix of size ($180 \times 1500 \times 8$).

Each trial was divided into non-overlapping windows of 125 samples ($250ms$). Five time-domain features were extracted from each window and channel: mean absolute value (MAV), variance, waveform length (WL), zero crossings (ZC), and slope sign change (SSC) [6], [48], [49], [50]. We excluded the final window for each trial to eliminate artifacts caused by the next phase of the trial. After feature extraction, the resulting data matrices are structured as (*trials* $\times$*windows*$\times$ *features*), where the feature vector has a length of 40 (5 features $\times$ 8 channels).

C. Visual Feedback Online Training

The participant with ULD was congenital, which made performing the set of five hand gestures (hand open, hand

close, wrist extension, wrist flexion, and rest) unintuitive, as they reported that they had never tried performing all those gestures with their impacted limb before. Therefore, we adapted the protocol to three gestures: hand open, hand close, and rest. Furthermore, upon receiving feedback from the participant that they require training time to reliably perform the three gestures, we developed a real-time visual training framework. Prior research has shown that decoder training, combined with targeted user feedback, enhances pattern separability through decoder-informed motor training and promotes motor skill retention through biofeedback [44], [51]. The participant followed randomized on-screen visual cues prompting each of the gestures (open, close, rest). For each cue, the participant performed three trials of 5 seconds with 6-second rest intervals, while moving the arm randomly. The participant was instructed to attempt the gestures with the residual limb in the same manner as with the intact contralateral limb to support motor imagery and control. A linear discriminant analysis (LDA) classifier was then trained on the recorded data to create the gesture-specific decision boundaries in the sEMG feature space. The participant received real-time feedback during training by visualizing the position of their sEMG features relative to the classifier boundaries.

D. Latent Representation Alignment via MCCA

We employed MCCA [42], [52] to address sEMG variability caused by changes in limb position, cross-day variability, and individual differences. The pre-processed sEMG data for each subject, day, or position is denoted as $X_n \in \mathbb{R}^{T\times d}$, where $n \in 1, 2, \ldots, N$, d is the number of features, and T is the number of datapoints from all concatenated trials. First, we concatenated the N datasets along the feature dimension to construct a global matrix:

$$X = [X_1 \mid X_2 \mid \cdots \mid X_N] \in \mathbb{R}^{T\times D} \tag{1}$$

where $D = N \times d$. We then computed the global block-diagonal covariance matrix $C \in \mathbb{R}^{D\times D}$ which captures both within- and between-dataset covariances. Each block diagonal of C was then individually whitened using principal component analysis (PCA), forming a block-diagonal whitening matrix $\tilde{X} \in \mathbb{R}^{D\times D}$, which was then used to whiten the global covariance matrix:

$$\tilde{C} = \tilde{X}^{\top} C \tilde{X} \in \mathbb{R}^{D\times D} \tag{2}$$

ensuring that all within-dataset covariances are decorrelated and scaled to unit variance, while the cross-dataset covariance structure was preserved. A second PCA was then applied to $\tilde{C}$ to extract dominant directions shared across datasets. We retained the top d° components to preserve only those patterns with the highest shared latent structure, yielding a projection matrix $\hat{V} \in \mathbb{R}^{D\times d^{\circ}}$. The final global transformation matrix was constructed as:

$$V = \tilde{X}\hat{V} \in \mathbb{R}^{D\times d^{\circ}} \tag{3}$$

which was used to project X into a common low-dimensional space that maximally captures the shared structure across the datasets. Additionally, dataset-specific transforms were obtained by partitioning V into N dataset-specific blocks:

$$V = \begin{bmatrix} V_1 \\ V_2 \\ \vdots \\ V_N \end{bmatrix}, \quad V_n \in \mathbb{R}^{d\times d^{\circ}}, n = 1 : N \tag{4}$$

Each dataset was then projected into the shared latent space using its corresponding transformation:

$$Y_n = X_n V_n \in \mathbb{R}^{T\times d^{\circ}} \tag{5}$$

The number of retained components (hereafter referred to interchangeably as Canonical Correlates, CCs) is estimated from the Summary Components (SCs), which are given by the columns of the projected data $Y = XV$. The leading SCs represent temporal patterns that capture most of the correlation across the data matrices X_n. The variance of these SCs ranges from 1 (no correlation) to N (perfect correlation across all N datasets), providing the basis for selecting a range of CCs. The optimal CC is determined by maximizing the decoding accuracy (Figure 4).

Plug-and-play functionality was achieved by estimating transformation matrices using one trial per gesture from a new condition (i.e., different limb position, day, or user). We constructed a calibration matrix of dimensions $T \times d$ by temporally repeating each trial to match the length of the reference dataset, ensuring both dimensional consistency and class correspondence required for alignment. This one-shot calibration aligned the acquired data in the new condition with a pre-trained model by mapping the new data into the reference feature space using the following equation [23]:

$$\hat{X}_{\text{test}} = X_{\text{test}} V_{\text{test}} V_{\text{ref}}^{\dagger} \in \mathbb{R}^{T\times d} \tag{6}$$

where † denotes the Moore–Penrose pseudo-inverse, and $\hat{X}_{test}$ is the projection of newly acquired data in the space spanned by features of training reference data.

E. Evaluation Framework

We evaluated classification accuracy under varying sEMG conditions using three strategies:

- **Baseline**: We established a performance baseline using an SVM model trained and tested using unaligned features.
- **Aligned**: We assessed how alignment affects decoding accuracy by projecting the reference and new data into a shared latent space using MCCA, in which training and classification occur (Figure 2).
- **Mapped**: New data are projected into the shared latent space, then mapped back into the reference feature space, and classified using the pretrained Baseline model, enabling one-shot learning (Figures 2, 3).

These strategies are applied across all alignment scenarios: cross-arm position, cross-day, and cross-subject.

1) Within-Session Alignment Across Arm Positions: The limb position effect is a major factor in degrading sEMG decoding performance. We investigated whether aligning latent representations of sEMG across different limb positions can uncover similar patterns of activity for different hand gestures.

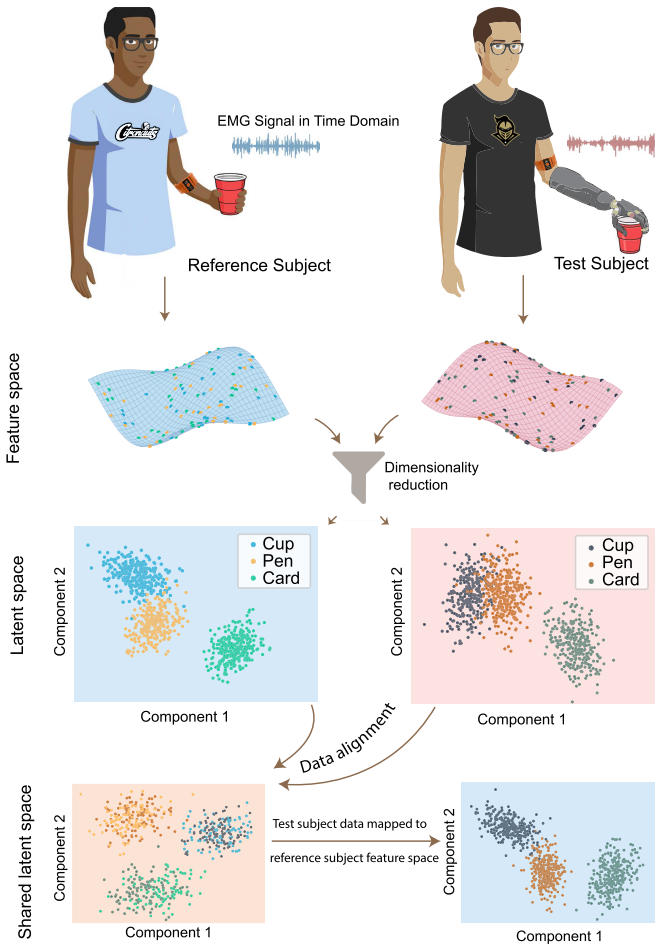

Fig. 2. Schematic of the alignment framework. sEMG signals were recorded from two subjects as they performed the same object tasks (e.g., holding a cup, pen, or card). Raw signals were transformed through feature extraction into high-dimensional feature spaces, which differed across individuals due to anatomical and physiological variability. Dimensionality reduction was then applied to project each subject's data into a lower-dimensional latent space, where class structure remained misaligned across subjects. Both subjects' data were projected into a shared latent space using MCCA, revealing shared latent representation across subjects. Alternatively, the test subject's data can be mapped directly into the reference subject's feature space for classification using a pretrained model on the reference data. The scatter plots illustrate the latent spaces before and after alignment, showing how data with distinct individual-specific structures can be projected into a common space that preserves class separability while minimizing cross-subject variability.

For these analyses, we only used the static mode sessions to minimize the impact of motion. Each session was preprocessed and arranged into a matrix of shape (240, 19, 40) (Section II-B). We reshaped the session data into a position-wise structure (16, 285, 40), corresponding to (*positions* $\times$*windows*$\times$ *features*). Within each session, $\binom{16}{2}$ position pairs were then evaluated. For each pair, the first position served as the reference (training) and the second as the test. Notably, one session from subjects 18 and 8 was excluded due to technical issues with Bluetooth connectivity. The transformation matrix was derived by applying MCCA to the reference and calibration data (one trial per gesture). Moreover, we compared classification performance across the three strategies: Baseline, Aligned, and Mapped.

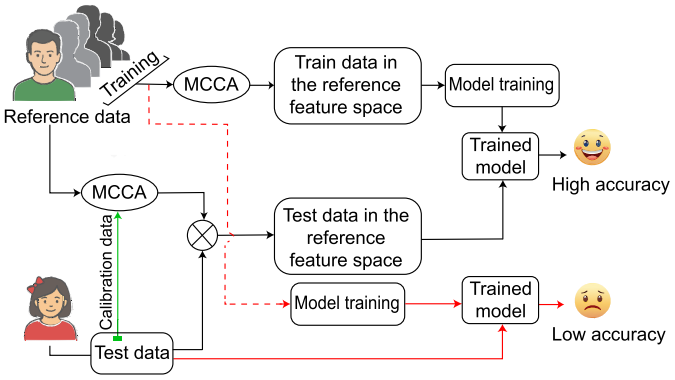

Fig. 3. Block diagram comparing the proposed plug-and-play (i.e., Mapped) strategy (black lines) with the Baseline strategy (red lines). Note that the model training in the Mapped strategy is a one-time effort, and no retraining is needed for test data. Calibration data is one trial per gesture from the test subject.

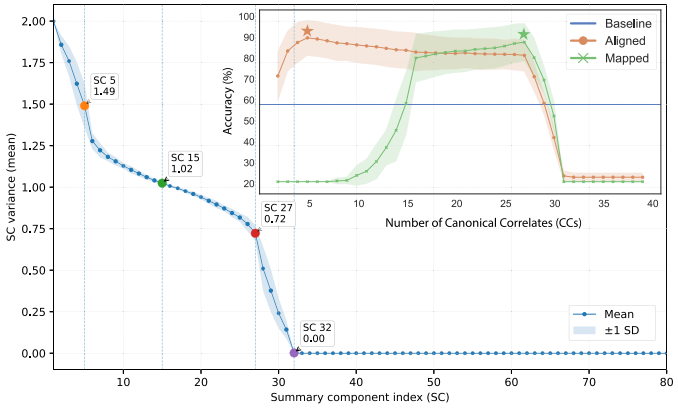

Fig. 4. An example of the effect of the number of Canonical Correlates (CCs) on decoding accuracy across different strategies. Classification accuracy is plotted as a function of the number of retained components for three evaluation strategies: **(1)** Baseline: the model is trained on session 1 (reference data) and evaluated on session 2 (test data) in their original feature space without alignment (blue); **(2)** Aligned: both reference and test data are projected into a shared latent space using MCCA, and classification is performed in this space (blue); **(3)** Mapped: test data are projected into the feature space of the reference data and classified using the Baseline model (green). Each curve shows mean accuracy across subjects; shaded areas denote standard deviation. (★) indicates the number of components selected for each strategy based on SC variance and statistical significance. Only one trial per gesture from the test session was used to estimate the MCCA transformation.

(1) Baseline (Unaligned Feature Space): An SVM_{Baseline} classifier with radial basis function (RBF) kernel and a regularization parameter of $C = 1.0$ was trained on the full feature matrix of the reference position and tested directly on the features of the test position, without any alignment.

(2) Aligned (Shared Latent Space): The reference and test datasets were aligned and projected into the shared latent space using the derived transformation matrix, using only the top 5 components for non-ULD subjects, and 3 for the ULD subject. The classifier, SVM_{Aligned}, was then trained on the aligned reference dataset and tested on the aligned new dataset within the shared latent space.

(3) Mapped (Reference Space): The test dataset was aligned with the reference dataset, projected into the shared latent space using the top 27 components for non-ULD subjects, and 29 for the ULD subject, and mapped back into the reference feature space using the pseudo-inverse of the reference

transformation matrix (Equation 6). The pretrained SVM_{Baseline} was then used to classify the mapped test dataset without retraining.

2) Within-Subject Cross-Day Alignment: Day-to-day variability in EMG signals is a critical complication for reliable myoelectric decoding. We evaluated whether the alignment framework can uncover consistent muscle activation patterns across days, using static sessions from 17 subjects (subject 18 was excluded due to technical issues) and dynamic sessions from 16 subjects (subjects 7 and 9 were excluded due to technical issues). For each subject, the first session was used as the reference (training) dataset and the second as the test dataset. As outlined in Section II-D, the calibration matrix was constructed using one trial per gesture from the test dataset ($\sim$ 2% of the data) and was then used to derive MCCA transformation matrix. We adopted the same Baseline, Aligned, and Mapped strategies as described in the previous subsection (Section II-E.1), with the only difference being the number of retained components. For non-ULD subjects, 5 components were retained for Aligned across both static and dynamic sessions, with 27 and 28 retained for Mapped in static and dynamic, respectively. In contrast, for the ULD subject, static sessions retained 3 components for Aligned and 26 for Mapped, whereas dynamic sessions retained 4 and 28.

3) Cross-Subject Alignment: Cross-subject variability presents a significant challenge for generalizable sEMG-based classification. To assess whether shared muscle activation patterns exist across subjects, we performed a cross-subject analysis using static and dynamic sessions separately. Each subject was iteratively selected as the reference, and the remaining subjects formed the test set. At each iteration, one additional subject (both sessions) was incrementally added to the training set, and evaluation was performed on the updated test set. This process continued until only one subject remained in the test pool. The inclusion of the training subjects was randomized in each iteration. This incremental approach assessed the robustness and scalability of the model. In particular, it allowed us to examine whether the alignment method can capture enough shared structure from a limited training set to generalize to unseen subjects, and analyze how adding more subjects to the training set impacts alignment performance and classification accuracy.

The calibration matrix was constructed using one trial per gesture from each test dataset, as described in Section II-D. For both projection into the shared latent space and inverse mapping to the reference space, 5 components were retained for analyses limited to non-ULD subjects. For analyses involving the ULD subject, the same incremental learning procedure was applied, with the test set being solely the ULD subject. In the ULD case, Aligned retained 3 components in both static and dynamic modes, while Mapped retained 28 components in static mode and 29 in dynamic mode. Performance was evaluated using the Baseline, Aligned, and Mapped strategies:

(1) Baseline (Unaligned Feature Space): An SVM classifier was trained on the training dataset features and evaluated on the test dataset features, without alignment.

(2) Aligned (Shared Latent Space): The calibration and training datasets were used to obtain the transformation matrix through MCCA. Both training and test datasets were then projected into the shared latent space, where the classifier was trained and evaluated.

(3) Mapped (Reference Space): In this method, the reference denotes the reference subject, which also serves as the initial training subject. Training subjects refer to those incrementally added to the training set, while test datasets correspond to the remaining subjects. The training subjects' datasets were aligned and projected into the shared latent space, then inverse-mapped into the reference subject's feature space, where the model was trained (Section II-D). The test subject's dataset was aligned with the reference subject's data using the calibration matrix, projected into the shared space, and inverse-mapped into the reference feature space before being classified using the pretrained model without retraining (Figure 3).

4) Cross-Subject Alignment in Object-Grasp Tasks: We extended our cross-subject analysis to object-grasp tasks to evaluate alignment performance in a more complex and dynamic motor control scenario. In our study, we selected three everyday objects (cup, pen, and card) because each typically elicits a distinct and functional grasp shape commonly used in daily life: power grasp, tripod grasp, and lateral grasp, respectively. Importantly, we did not constrain participants to perform a specific grasp shape for each object. Instead, they were free to grasp the objects in their own natural way. This was designed to decode the user's intention to grasp the object naturally and investigate the inter-subject variability in muscle activation patterns in object-grasping tasks. Subject 4 was excluded from this analysis due to technical issues with the collected data. We adopted the same incremental training strategy described in the previous subsection (Section II-E.3).

F. Statistical Analysis

Statistical analysis was performed in Python using the SciPy and StatsModels libraries to compare classification accuracy across the aforementioned strategies. First, the Shapiro–Wilk test was used to evaluate the data's normality. If the data followed a normal distribution, a paired t-test was conducted; otherwise, the Wilcoxon signed-rank test was used for non-parametric comparison. All p-values were corrected for multiple comparisons using the Bonferroni method. In addition to significance testing, effect sizes were reported as Cohen's d for t-tests and rank-biserial correlation r for Wilcoxon tests. We quantified class separability on the Riemannian manifold of covariance matrices. Trial-wise covariance matrices were estimated using Ledoit–Wolf regularization, class centers were computed with the Fréchet mean, and geodesic distances were evaluated using the Affine Invariant Riemannian (AIR) distance. Intra-class distances were defined by the Centroid Diameter Distance, and inter-class distances by the Centroid Linkage Distance.

III. Results

A. MCCA Reveals Position-Invariant Muscle Activation Patterns

The accuracy of hand gesture recognition using sEMG is degraded when the same gesture is performed at a different arm position from the one on which the decoder was trained.

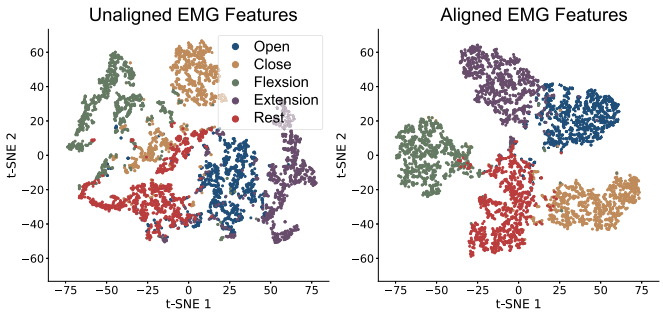

Fig. 5. MCCA alignment improves class clustering by reducing the limb position effect. Visualization of sEMG features projected into a two-dimensional t-SNE space from one session in static mode for all 16 arm positions. **left:** sEMG feature distribution before alignment in the original feature space in static mode, where samples of the same gesture appear scattered due to the influence of limb position on muscle activity. **right:** sEMG feature distribution after MCCA alignment showing clear clustered data illustrating that alignment mitigates position-induced variability while preserving gesture-specific structure.

This phenomenon, known as the limb position effect, is believed to be due to position-induced variability in muscle coordination and, hence, different muscle activity patterns. To confirm the existence of such an effect in our dataset, we trained and tested an SVM classifier on the same arm position and obtained a high decoding accuracy for both non-ULD (90.151% ± 9.413) and ULD (91.588% ± 7.674) groups. In contrast, when we trained the classifier on one arm position and tested on another, the accuracy dropped to 80.160% ± 15.546 and 85.210% ± 11.809, respectively. This 7-10% reduction in performance highlights the impact of the limb position effect on decoding accuracy in both groups and motivates the need for position-invariant strategies. Building on this observation, we hypothesized that there exists a shared latent structure that underlies each gesture regardless of limb position and that alignment through MCCA can unveil these latent structures. To illustrate, we examined a session in static mode, where gestures were performed at fixed limb positions. The unaligned sEMG features were then projected into a two-dimensional space using t-SNE. The visualization revealed highly scattered gesture clusters across 16 arm positions pre-alignment (Figure 5, left). However, after MCCA alignment, data exhibited a well-defined cluster distribution (Figure 5, right), thereby potentially improving decoding performance.

After visually observing that MCCA effectively captured shared patterns across arm positions, we subsequently quantified its impact on classification accuracy across arm positions using an SVM model. First, we assessed the model performance of the Baseline strategy, followed by the Aligned strategy (Figure 6A, G). For non-ULD subjects, we found that the model trained in the shared latent space achieved an 8% increase in accuracy compared to the Baseline (Baseline: $mean \pm std$: 80.160% ± 15.546, Aligned: $mean \pm std$: 88.212% ± 8.953, Wilcoxon signed-rank test: $p \approx 0.0, r = 0.637$; Figure 6A). Importantly, a similar improvement was observed for the ULD subject (Baseline: $mean \pm std$: 85.210% ± 11.809, Aligned: $mean \pm std$: 89.186% ± 8.570, Wilcoxon signed-rank test: $p = 5.712 \times 10^{-14}, r = 0.5264$; Figure 6G), confirming that the alignment framework generalizes robustly to both non-ULD and ULD subjects.

Although we observed increased accuracy by projecting both reference and test datasets to the shared latent space, this technique requires retraining the classifier in this latent space. This retraining causes a practical burden for activities of daily living in which the arm positions can be held in an infinite different positions. Therefore, we examined whether the classifier trained on the reference arm position can be used without retraining alongside the MCCA alignment strategy to obtain a high classification accuracy for the test arm position using the Mapped strategy (Section II-D). We found that the Mapped strategy increased the accuracy by 2% on average across all arm position combinations compared to the Baseline strategy. This improvement was observed consistently across both groups, non-ULD subjects (Baseline: $mean \pm std$: 80.160% ± 15.546, Mapped: $mean \pm std$: 82.442% ± 12.843, Wilcoxon signed-rank test: $p = 3.996 \times 10^{-18}, r = 0.174$; Figure 6A), and the ULD subject (Baseline: $mean \pm std$: 85.210% ± 11.809, Mapped: $mean \pm std$: 87.220% ± 9.757, Wilcoxon signed-rank test: $p = 2.258 \times 10^{-5}, r = 0.3366$; Figure 6G). These analyses demonstrate the effectiveness of MCCA in reducing the limb position effect as evidenced by improved classification accuracy across different arm positions, both using Aligned and Mapped strategies.

B. Alignment Compensating for Cross-Day EMG Variability

We showed that aligning the latent representation of sEMG features reduced the limb position effect. However, it is unclear whether the same technique could be used to develop robust classifiers across recording days where muscle activity patterns can vary due to several factors such as electrode shift, device adaptation, fatigue, or other neuromuscular changes. To evaluate this, we analyzed two recording sessions of the same subject to determine whether MCCA could find a strong shared muscle activation pattern across different days. Our initial analysis focused on static mode, where subjects performed the same gesture for 5 seconds at fixed arm positions. To quantify cross-day variability, we first trained and tested the model on the same session, resulting in high within-session performance with average accuracies of 90.081% ± 7.969 for the non-ULD subjects and 90.967% ± 6.113 for the ULD subject. In contrast, the Baseline model, trained on the first session and tested on the second, achieved an accuracy of 56.143% ± 24.767 for non-ULD subjects (Figure 6B), and 65.278% for the ULD subject, corresponding to degradations of 33.94% and 25.7%, respectively, caused by cross-day variability. Therefore, we next applied alignment for cross-day data to examine whether alignment can improve the accuracy across days. We found that training the classifier in this shared latent space significantly improved accuracy in non-ULD subjects by 27.29% compared to the Baseline (Baseline: $mean \pm std$: 56.143% ± 24.767, Aligned: $mean \pm std$: 83.430% ± 11.505, Wilcoxon signed-rank test: $p = 9.156 \times 10^{-5}, r = 0.855$; Figure 6B). Similarly, for the ULD subject, accuracy improved by 25% after alignment (Baseline: 65.278%, Aligned: 90.351%). Interestingly, these improvements nearly offset the reductions observed in the initial cross-day variability test,

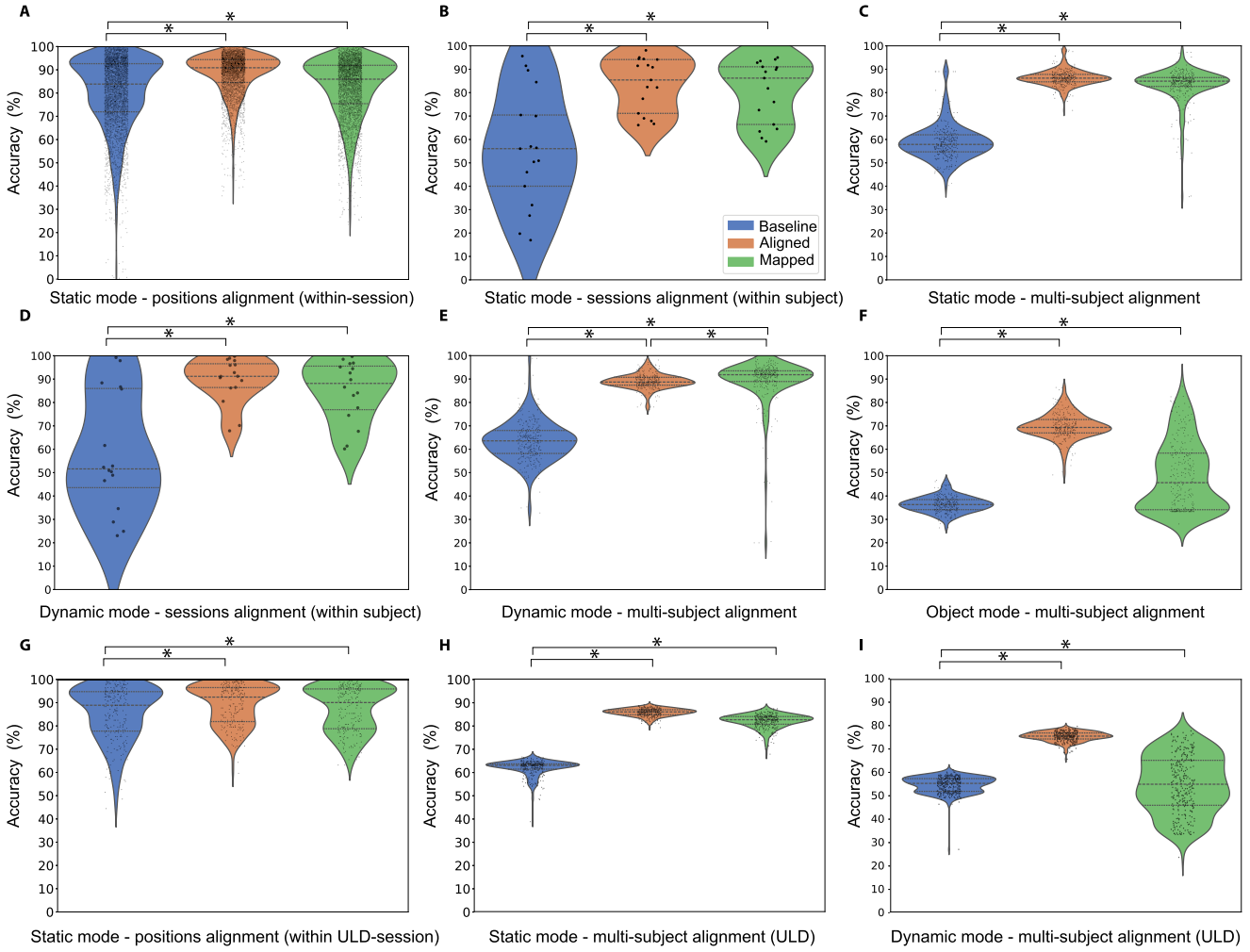

Fig. 6. MCCA alignment improves EMG decoding across different experimental conditions with minimal calibration. Each panel shows classification accuracy distributions under three evaluation strategies: Baseline (blue), Aligned (orange), and Mapped (green), following the notation introduced in Figure 4. The MCCA transformation was estimated using one trial per gesture from the test set. (*) denotes statistically significant differences (Bonferroni-corrected $p < 0.05$, using paired t-test or Wilcoxon signed-rank test). Dashed lines indicate the 25th, 50th (median), and 75th percentiles. The first two rows show the non-ULD subject's results, and the last row shows results for the congenital ULD subject. **A, G)** Within-session cross-arm position classification under static mode, using arm position pairs where one arm position serves as the training (reference) and the other as the test. **B, D)** Within-subject cross-days session alignment for static and dynamic modes, respectively; the first session is used for training (reference) and the second for testing. **C, E, F, H, I)** Cross-subject classification in static, dynamic, and object-grasping modes, respectively, using incremental subject alignment; Each subject is sequentially added to the reference set, and a new model is incrementally trained by adding aligned subjects, reducing the test set until only one subject remains. In the ULD case, the same incremental training strategy was used, with ULD data as the test set. Session modes referenced here are described in the task protocol (Figure 1B).

demonstrating that even minimal calibration data can substantially reduce the effect of cross-day recording variability through alignment.

Similar to the analysis across arm positions, projecting the cross-day data to the shared latent space requires retraining the classifier, increasing the training burden. Therefore, we examined whether the Mapped strategy would result in robust classification across days. This approach yielded a 24.25% improvement in classification accuracy compared to the Baseline for non-ULD subjects (Baseline: $mean \pm std$: $56.143\% \pm 24.767$, Mapped: $mean \pm std$: $80.396\% \pm 13.252$, Wilcoxon signed-rank test: $p = 5.798 \times 10^{-4}, r = 0.798$; Figure 6B), and by 26% in the ULD subject (Baseline: 65.278%, Mapped: 91.338%). Beyond improving accuracy, the Mapped strategy offers a practical advantage by enabling direct application of pre-trained models, facilitating real-time implementation without additional training.

Having demonstrated that alignment effectively captures shared structure across days in static gestures for both ULD and non-ULD subjects, we next evaluated its impact in dynamic mode, where subjects performed the same gestures while simultaneously moving their hands between positions. Unlike the static sessions, where arm position remains fixed, dynamic gestures introduce additional complexity due to movement inconsistency across days. To confirm the effect of cross-day variability in the dynamic mode, we trained and tested an SVM classifier within the same day and compared performance to the Baseline model, trained on day 1 and tested on day 2. Non-ULD subjects achieved an accuracy of $94.271\% \pm 5.629$, showing an increase of 35.97% compared to the Baseline ($mean \pm std$: $58.302\% \pm 25.708$). Similarly, the ULD subject achieved an accuracy of $81.019\% \pm 9.987$, an increase of 27.58% compared to the Baseline (53.439%).

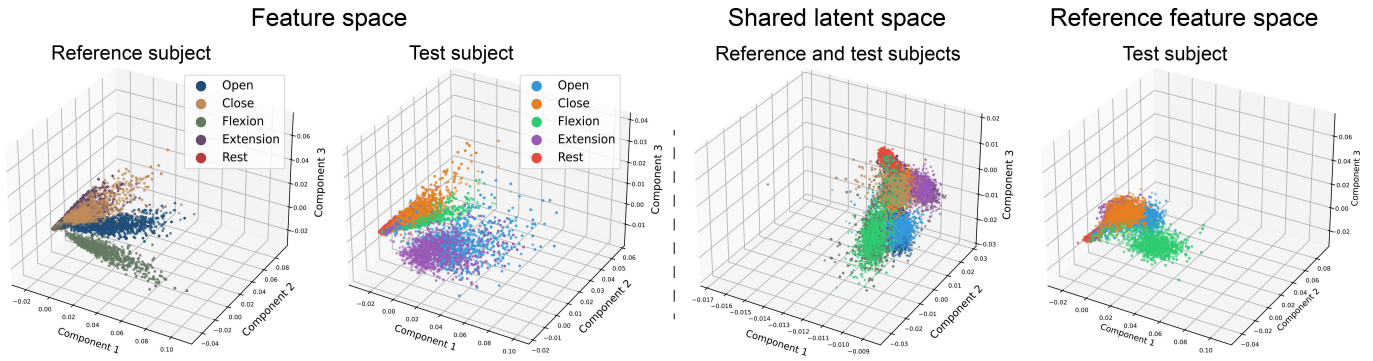

Fig. 7. Cross-subject alignment using MCCA enhances class-wise consistency. Data from a reference and test subject are shown in three spaces to illustrate the effect of MCCA. **Left two panels:** PCA of the reference and test subjects' feature spaces highlights class-specific structure and cross-subject variability. **Middle-right:** In the shared latent space, data from both subjects are well-aligned with class clusters closely overlapping, indicating strong class-wise correspondence. **Rightmost:** Test subject data mapped back to the reference subject's feature space recovers a structure closely resembling the reference distribution (the left panel), demonstrating effective mapping.

Despite the increased complexity during dynamic mode, alignment remained highly effective. Projecting both training and test data into the shared latent space led to a 31.29% improvement over the Baseline for non-ULD subjects (Baseline:$mean \pm std$: 58.302%±25.708, Aligned: $mean \pm std$: 89.590% ± 9.627, Wilcoxon signed-rank test: $p = 3.052 \times 10^{-4}, r = 0.840$; Figure 6D), and a 15.15% improvement compared to the Baseline for the ULD subject (Baseline: 53.439%, Aligned: 68.598%). Similarly, mapping test data onto the reference feature space that removes the need to retrain a classifier improved accuracy by 26.62% for non-ULD subjects (Baseline:$mean \pm std$: 58.302% ± 25.708, Mapped: $mean \pm std$: 84.921% ± 13.147, t-test: $p = 6.487 \times 10^{-4}, d = 1.159$; Figure 6D), and by 6% for the ULD subject (Baseline: 53.439%, Mapped: 59.444%). Notably, this advantage was not dependent on the order of days, as we achieved similar levels of accuracy if the second day was used as the reference instead (data not shown).

C. Mitigating Cross-Subject Differences in EMG Characteristics

Now that we have established that alignment of muscle activity latent representation effectively mitigates both limb position effect and cross-days variability, we next investigated whether this approach could also reduce the effect of individual differences and enhance cross-subject generalization. In particular, we wanted to assess whether a classifier trained on non-ULD subjects could generalize to the ULD subject, a challenging case given substantial differences in muscular physiology and activation patterns. Notably, for non-ULD subjects, intra-subject classification achieved high accuracy in both static (89.717% ± 6.977) and dynamic (92.733% ± 7.435) modes, compared to cross-subject classification, which reached only (57.913% ± 7.885) in static and (58.302% ± 25.708) in dynamic mode. For the ULD subject, intra-subject accuracy was 90.14% (static) and 78.043% (dynamic). In contrast, training the classifier on non-ULD subjects and testing on the ULD subject reduced accuracy to 61.795% ± 3.382 in static and to 54.699%±3.647 in dynamic mode. This reduction in decoding accuracy reflects the inter-subject variabilities.

To better understand the impact of alignment on cross-subject generalization, we aligned the static-mode data from two non-ULD subjects and projected them into a shared latent space. As shown in Figure 7, the 3D visualization reveals the relative geometry of the two subjects and illustrates how alignment reduces inter-subject discrepancies. The test and reference subjects exhibited distinct class-specific distributions in their original feature space. After alignment, however, the data from both subjects became highly correlated, with considerable overlap in class distributions. Furthermore, when mapping the test subject data from the shared space back into the reference subject's feature space, the test data closely resembled that of the reference subject. Quantitative analysis substantiated the visual trends in Figure 7. We compared cross-subject intra-class and inter-class Riemannian distances (Section II-F) before and after mapping to the reference space. Our analysis revealed that mapping the test subject into the reference space reduced within-class spread by 78% (d_{intra} : 7.06 → 1.56), while preserving relatively large between-class separation (d_{inter} : 15.52 → 9.94), thereby enhancing overall class discriminability. We next evaluated whether this effect would hold if the test subject was an individual with ULD. We found that after mapping the ULD subject to the non-ULD subject feature space, within-class spread slightly decreased (d_{intra} : 2.55 → 2.3), while between-class separation nearly doubled (d_{inter} : 7.5 → 13.08). Together, these results indicate that the Mapped strategy reduces cross-subject variability and results in more compact, well-separated clusters, even when subjects differ substantially in muscular physiology.

The same strategy also showed promising results for the dynamic mode. More specifically, two subjects were chosen to examine how their sEMG pattern activity evolved over time in their feature space as the arm was moving. Figure 8 depicts the resulting temporal trajectories for each hand gesture before and after alignment. The aligned trajectories showed reduced subject-specific variability while preserving the temporal structure of each gesture.

To quantitatively evaluate the cross-subject alignment effect on hand gesture recognition, we applied the incremental learning approach (Section II-E.3). We then compared classifier performance across the three aforementioned strategies: Baseline, Aligned, and Mapped. In the static mode, cross-subject alignment using both Aligned and Mapped strategies showed an increase in classification accuracy com-

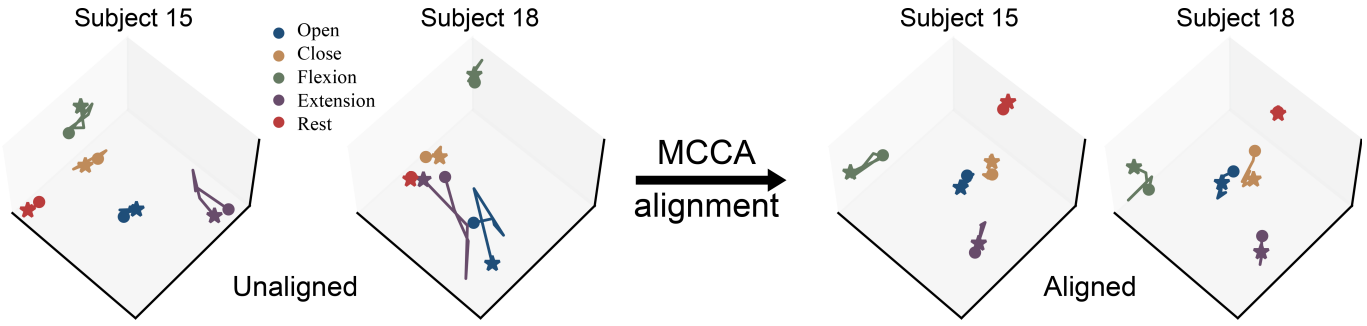

Fig. 8. Three-dimensional representation of the muscle activity latent dynamics for two subjects in dynamic mode before and after alignment with MCCA. (★) indicates the start of movement, and (•) indicates the end of movement while performing a gesture. PCA was used to capture the latent dynamics of movement execution, followed by MCCA for spatial alignment. Each trajectory reflects the temporal evolution of EMG features during hand gestures as the subject's arm transitions between positions, averaged across trials. Before alignment **(left)**, distinct subject-specific variability is evident. After alignment **(right)**, the gesture trajectories across subjects are well-aligned, demonstrating a reduction in cross-subject variability while maintaining the underlying temporal dynamics of the gestures.

pared to the Baseline. More specifically, for non-ULD subjects, the model trained in shared latent space increased accuracy by 28.09% compared to the Baseline (Baseline: $mean \pm std$: 57.913% ± 7.885, Aligned: $mean \pm std$: 86.003% ± 3.113, Wilcoxon signed-rank test: $p \approx 0.0, r = 0.867$; Figure 6C). Importantly, alignment also improved cross-subject generalization from non-ULD subjects to the ULD subject by a 23.8% accuracy increase (Baseline: $mean \pm std$: 61.795% ± 3.382, Aligned: $mean \pm std$: 85.675% ± 1.638, Wilcoxon signed-rank test: $p \approx 0.0, r = 0.867$; Figure 6H).

Furthermore, the Mapped strategy increased accuracy for non-ULD subjects by 23.708% (Baseline: $mean \pm std$: 57.913% ± 7.885, Mapped: $mean \pm std$: 81.621% ± 9.845, Wilcoxon signed-rank test: $p \approx 0.0, r = 0.835$; Figure 6C). Notably, the model pre-trained on non-ULD subjects generalized well to the ULD subject, increasing accuracy by 20.1% (Baseline: $mean \pm std$: 61.795% ± 3.382, Mapped: $mean \pm std$: 81.932% ± 3.030, Wilcoxon signed-rank test: $p \approx 0.0, r = 0.867$; Figure 6H). Although both strategies significantly improved decoding, Aligned accuracy was 4.38% and 3.8% higher than Mapped for non-ULD and ULD subjects, respectively. Nevertheless, as previously noted, mapping back the test subject data to the reference subject feature space eliminates the need to retrain the classifier.

In the dynamic mode, without alignment (i.e., Baseline strategy), the classification accuracy was 63.446% ± 8.550 for non-ULD subjects and 54.699% ± 3.647 for ULD. However, aligning training and test data in a shared latent space significantly improved the mean accuracy by 25.55% for non-ULD subjects (Baseline: $mean \pm std$: 63.446% ± 8.550, Aligned: $mean \pm std$: 88.997% ± 3.166, Wilcoxon signed-rank test: $p \approx 0.0, r = 0.867$; Figure 6E), and by 23.04% for ULD (Baseline: $mean \pm std$: 54.699% ± 3.647, Aligned: $mean \pm std$: 77.743% ± 1.488, Wilcoxon signed-rank test: $p \approx 0.0, r = 0.867$; Figure 6I). The reduction in standard deviation indicated reduced variability across subjects. Importantly, projecting test data directly into the reference subject's feature space achieved a comparable accuracy 88.982% for non-ULD subjects, though with higher variability (Aligned: $mean \pm std$: 88.997% ± 3.166, Mapped: $mean \pm std$: 88.982% ± 10.484, Wilcoxon signed-rank test: $p = 4.365 \times 10^{-16}, r = 0.472$; Figure 6E). The Mapped strategy also improved Baseline model accuracy by 19.7% when tested on the ULD subject (Baseline: $mean \pm std$: 54.699% ± 3.647, Mapped: $mean \pm std$: 74.399% ± 2.521, Wilcoxon signed-rank test: $p \approx 0.0, r = 0.867$; Figure 6I). Collectively, these results establish MCCA-based alignment as a powerful approach for cross-subject generalization, supporting accurate and reliable decoding of dynamic sEMG signals despite pronounced inter-subject heterogeneity, movement, and recording variability.

D. Reducing Cross-Subject Variability in Object-Grasping Tasks

Having validated that alignment of sEMG latent space representations effectively reduced variability across limb positions, days, and subjects, we next investigated whether this approach could generalize to a more complex and naturalistic motor task: real-life object grasping during dynamic motion in which the participants are allowed to choose their preferred grasp. This is critical for developing intuitive myoelectric control, where the goal is to decode grasp intention despite individual differences in hand–object interaction, as both object properties and user grasp intention influence the hand shape. Indeed, subjects showed individual differences even for grasping similar objects. More specifically, when the model was trained and tested within the same subject, it achieved an average accuracy of 82.579% ± 9.683. However, accuracy dropped by 46.2% when tested on a different subject.

Therefore, we assessed whether MCCA-based alignment could uncover shared representations across non-ULD subjects performing an object-grasping task while moving between positions. We found that training on the aligned latent representations in the shared space led to a substantial improvement in classification accuracy compared to the Baseline strategy, with an average accuracy increase of 33.4% (Baseline: $mean \pm std$: 36.409% ± 3.429, Aligned: $mean \pm std$: 69.817% ± 5.448, Wilcoxon signed-rank test: $p \approx 0.0, r = 0.867$; Figure 6F).

Furthermore, mapping the test subject data into the training subject's feature space also improved performance, yielding a 12.08% increase in accuracy (Baseline: $mean \pm std$: 36.409% ± 3.429, Mapped: $mean \pm std$: 48.491% ± 14.561, Wilcoxon signed-rank test: $p = 3.08 \times 10^{-24}, r = 0.620$;

Figure 6F). While both alignment strategies enhanced generalization, training in the shared space resulted in a significantly larger and more consistent improvement across subjects. However, regardless of the strategy, the lower overall accuracy across both strategies highlights the difficulties in decoding more naturalistic grasps.

IV. Discussion

We evaluated our proposed alignment-based framework across three settings: cross-arm position, cross-day, and cross-user. These evaluation scenarios reflect the primary sources of variability in sEMG signals, including the limb position effect, temporal variability such as electrode shift, and individual differences [53]. We aimed to uncover an underlying shared structure preserved across these factors through alignment using MCCA [52].

Our results demonstrate that using a single trial per gesture for calibration, alignment using MCCA consistently improved classification accuracy of 5 hand gestures across 16 arm positions, recording days, and subjects (including ULD subject), and for 3 object-grasping tasks across subjects (Figure 6).

We first analyzed the impact of alignment on reducing the limb position effect and found that alignment-based strategies increased the accuracy, suggesting that MCCA identified a position-invariant structure that preserves gesture-relevant muscle activity. Similar results were reported by Cheng et al. [19], who observed a substantial 44.19% increase in accuracy using CCA to reduce the limb position effect. These results reinforce the hypothesis that limb position primarily modulates muscle recruitment patterns, rather than the underlying movement intent, as demonstrated by the improvement in accuracy using alignment. Therefore, aligning sEMG signals across limb positions recovers a shared representation of motor intent that is resilient to biomechanical variations.

Next, we evaluated alignment across recording days, which introduces temporal variability such as electrode shift. In both static and dynamic sessions, MCCA significantly improved classification accuracy, compensating for electrode shifts and temporal perturbations that occur across days. Our findings are consistent with those of Donati et al. [23], who reported a within-subject average accuracy of 95% when generalizing an SVM model trained on Day 1 recordings to new sessions collected over a 10-day period using two trials per gesture for calibration. In their study, electrode placement was not controlled, which supports our hypothesis that alignment can reduce the impact of electrode shifts. However, their reported accuracy is 14.6% higher than ours (80.4%), possibly due to the added complexity in our experiment, including 16 arm positions (as opposed to no arm position variations) and the use of only one calibration trial (as opposed to two) per gesture.

We further investigated whether alignment could reduce cross-subject variability in muscle activation patterns and generalize to a participant with a congenital limb difference. Our results indicated that alignment substantially improved cross-subject generalization. These findings align with related work by Xue et al. [12], who applied CCA and reported a 39.73% increase in accuracy, reaching 69.66%, and further improved performance to 78.15% using domain adaptation. Wang et al. [13] combined Discriminative CCA (DCCA) with Adaptive Dimensionality Reduction (ADR) to classify 12 upper-limb movements across 8 subjects, achieving 90.52% accuracy. Although their reported accuracy exceeds ours by 9% in static mode and 1.6% in dynamic mode, this gap might be due to the differences in the evaluation setup. Their method used pairwise alignment and retrained a classifier for each test–train subject pair. In contrast, our framework aligns all subjects into a reference space, eliminating the need for retraining when adapting to new subjects.

Moreover, while most existing cross-subject decoding studies rely on deep neural networks or large-scale datasets [31], [54], our approach achieves generalization using only a single calibration trial per class by leveraging statistical alignment via MCCA and a pre-trained linear SVM classifier. Furthermore, our analysis revealed that data from as few as four subjects was sufficient to reach robust decoding performance (Baseline: $mean \pm std$: 55.1% $\pm$ 2.1, Mapped: $mean \pm std$: 84.6% $\pm$ 1.6). Together, these findings support the effectiveness of alignment in improving cross-subject decoding and suggest that aligning the latent structure of muscle activity can compensate for individual anatomical and physiological differences. Furthermore, we extended our analysis to generalize models trained on non-ULD participants to a participant with a congenital limb difference. Despite the likely recruitment of different muscle groups, alignment improved decoding accuracy by $\approx$ 20% in both static and dynamic modes. To our knowledge, this is one of the first demonstrations that a single trial per gesture can restore control performance in a congenital limb-difference participant to near non-ULD levels. Notably, the optimal components for the ULD participant differed from those without ULD. This difference may be attributable to differences in kinesthetic motor imagery when attempting gestures with a limb never possessed [55], [56].

Interestingly, decoding accuracy was consistently higher in the dynamic mode than in the static mode for non-ULD subjects. This finding is consistent with our earlier work [45], where we demonstrated that dynamic training is advantageous when the device is expected to operate predominantly under movement. Moreover, Radmand et al. [57] reported that dynamic training is as robust to limb position effects as training across multiple positions. In contrast, the ULD participant showed lower accuracy in the dynamic mode, which may be attributable to increased fatigue and the greater difficulty of performing the task, as reported by the participant.

Notably, because our analyses were restricted to within-mode evaluations, differences in trial count did not bias the reported results. However, cross-mode analyses must be bounded by both the number of trials and the positions included [45].

Finally, we validated our method on the object-grasping task across subjects. This task posed the highest level of complexity due to the combined effects of individual differences and additional variability introduced by arm movement, as each object was grasped and moved across multiple positions. Our results showed an average accuracy of 48.5% when using one-shot calibration for a pretrained model,

indicating difficulties decoding the object grasp intention. This is comparable to related work from Le et al. [22], who reported cross-day accuracies of 61% and 60% for large diameter (cup) and tripod (pen) grasps, respectively, when training and testing were conducted in the same arm position and within the same subject. One possible explanation for the poor generalizability in the object-grasping task is the heterogeneous muscle activation patterns from individual grasping techniques, suggesting that MCCA was likely unable to extract a sufficiently shared structure due to high cross-subject variability. Moreover, performance drop may be partially attributed to using non-standardized grasping instructions during our data collection, as the task was designed to preserve natural individual differences. Indeed, prior studies showed significant variability of individuals grasping objects differently, particularly for objects like pens [58].

Overall, our findings suggest that MCCA can extract high-level motor representations that persist across different arm positions, days, and subjects. Given the hierarchical nature of motor control, where sEMG activity reflects upstream neural commands, this shared representation may capture a common motor intent modulated by biomechanical and physiological factors. Similar patterns have been observed in electroencephalogram (EEG) studies, where shared latent dynamics are preserved across time and individuals [59], [60]. We hypothesize that sEMG signals may similarly encode an invariant structure, with observed variations reflecting how the underlying motor intention is adapted to different musculoskeletal configurations.

Notably, we observed that most task-relevant information is retained in just the top 5 CCs, suggesting that the underlying structure resides within a compact low-dimensional manifold, facilitating real-time inference while supporting model interpretability. In contrast, reconstructing the sEMG feature space using the Mapped strategy needed more components to retain (Fig. 4), possibly to account for condition-specific variability resulting from differences in electrode location, biomechanics, and muscle activation patterns. Despite the effectiveness of the proposed framework, several limitations remain. Although the model trained on aligned data in the shared latent space yields the highest classification accuracy, it requires retraining when new conditions are introduced, limiting its utility in real-time applications. In contrast, the Mapped strategy eliminates retraining by projecting new data into a reference space. However, this comes at the cost of reduced accuracy due to the potential reintroduction of condition-specific noise. Bridging this trade-off remains an important area to investigate in future work.

A promising future direction is to explore continual learning adaptive models using unsupervised online or few-shot alignment approaches. In addition, dynamic selection of the number of retained components may enhance robustness across varying acquisition conditions. Furthermore, building on our experimental results from a participant with a congenital limb difference, a key future direction for translating this approach to prosthetic control is to conduct closed-loop experiments with a larger population of individuals with upper-limb differences to establish clinical feasibility and generalizability.

V. Conclusion

We demonstrated that a one-shot alignment framework using MCCA can reliably extract shared latent representations of muscle activity across limb positions, days, and users, including a participant with a congenital upper limb difference. By aligning sEMG signals into a common latent subspace, our method resulted in accurate and generalizable decoding of gestures and object grasps with minimal calibration. These findings suggest that variability in sEMG across different conditions may reflect structured projections of a consistent motor intent rather than noise, and that this structure can be recovered through alignment. The proposed framework offers user-independent, calibration-efficient control suitable for wearable muscle-machine interfacing. Future work focusing on unsupervised adaptation and validation for prosthetic applications will be pivotal towards the wide deployment of the framework.

Acknowledgment

Article processing charges were provided in part by the UCF College of Graduate Studies Open Access Publishing Fund.

References

[1] P. K. Artemiadis and K. J. Kyriakopoulos, "An EMG-based robot control scheme robust to time-varying EMG signal features," *IEEE Trans. Inf. Technol. Biomed.*, vol. 14, no. 3, pp. 582–588, May 2010.

[2] A. Stoica, F. Salvioli, and C. Flowers, "Remote control of quadrotor teams, using hand gestures," in *Proc. 9th ACM/IEEE Int. Conf. Hum.-Robot Interact. (HRI)*, Mar. 2014, pp. 296–297.

[3] J. Kim, S. Mastnik, and E. André, "EMG-based hand gesture recognition for realtime biosignal interfacing," in *Proc. 13th Int. Conf. Intell. user Interfaces*. New York, NY, USA: Association for Computing Machinery, Jan. 2008, pp. 30–39, doi: 10.1145/1378773.1378778.

[4] X. Zhang, X. Chen, W.-H. Wang, J.-H. Yang, V. Lantz, and K.-Q. Wang, "Hand gesture recognition and virtual game control based on 3D accelerometer and EMG sensors," in *Proc. 14th Int. Conf. Intell. user Interface*, Feb. 2009, pp. 401–406.

[5] H. Koskimäki, P. Siirtola, and J. Röning, "Myogym: Introducing an open gym data set for activity recognition collected using myo armband," in *Proc. ACM Int. Joint Conf. Pervasive Ubiquitous Comput. Proc. ACM Int. Symp. Wearable Comput.*, Aug. 2017, pp. 537–546.

[6] X. Jiang, C. Ma, and K. Nazarpour, "Posture-invariant myoelectric control with self-calibrating random forests," *Frontiers Neurorobotics*, vol. 18, Dec. 2024, Art. no. 1462023.

[7] E. Eddy, E. J. Scheme, and S. Bateman, "A framework and call to action for the future development of EMG-based input in HCI," in *Proc. Conf. Hum. Factors Comput. Syst. (CHI)* New York, NY, USA: Association for Computing Machinery, Apr. 2023, pp. 1–23, doi: 10.1145/3544548.3580962.

[8] E. Eddy, E. Campbell, S. Bateman, and E. Scheme, "EMG-based wake gestures eliminate false activations during out-of-set activities of daily living: An online myoelectric control study," *J. Neural Eng.*, vol. 22, no. 1, Feb. 2025, Art. no. 016006.

[9] H. Xu and A. Xiong, "Advances and disturbances in sEMG-based intentions and movements recognition: A review," *IEEE Sensors J.*, vol. 21, no. 12, pp. 13019–13028, Jun. 2021.

[10] I. Kyranou, K. Szymaniak, and K. Nazarpour, "EMG dataset for gesture recognition with arm translation," *Sci. Data*, vol. 12, no. 1, p. 100, Jan. 2025.

[11] J. Hussain, K. Sundaraj, Y. F. Low, L. C. Kiang, S. Sundaraj, and M. A. Ali, "A systematic review on fatigue analysis in triceps brachii using surface electromyography," *Biomed. Signal Process. Control*, vol. 40, pp. 396–414, Feb. 2018.

[12] B. Xue et al., "Multiuser gesture recognition using sEMG signals via canonical correlation analysis and optimal transport," *Comput. Biol. Med.*, vol. 130, Mar. 2021, Art. no. 104188.

[13] J. Wang, D. Cao, Y. Li, J. Wang, and Y. Wu, "Multi-user motion recognition using sEMG via discriminative canonical correlation analysis and adaptive dimensionality reduction," *Frontiers Neurorobotics*, vol. 16, Oct. 2022, Art. no. 997134.

[14] M. Jochumsen, A. Waris, and E. N. Kamavuako, "The effect of arm position on classification of hand gestures with intramuscular EMG," *Biomed. Signal Process. Control*, vol. 43, pp. 1–8, May 2018.
[15] A. Fougner, E. Scheme, A. D. C. Chan, K. Englehart, and Ø. Stavdahl, "Resolving the limb position effect in myoelectric pattern recognition," *IEEE Trans. Neural Syst. Rehabil. Eng.*, vol. 19, no. 6, pp. 644–651, Dec. 2011.
[16] S. A. Stuttaford, M. Dyson, K. Nazarpour, and S. S. G. Dupan, "Reducing motor variability enhances myoelectric control robustness across untrained limb positions," *IEEE Trans. Neural Syst. Rehabil. Eng.*, vol. 32, pp. 23–32, 2024.
[17] Y. Teh and L. J. Hargrove, "Understanding limb position and external load effects on real-time pattern recognition control in amputees," *IEEE Trans. Neural Syst. Rehabil. Eng.*, vol. 28, no. 7, pp. 1605–1613, Jul. 2020.
[18] M. Jabbari, R. N. Khushaba, and K. Nazarpour, "EMG-based hand gesture classification with long short-term memory deep recurrent neural networks," in *Proc. 42nd Annu. Int. Conf. IEEE Eng. Med. Biol. Soc. (EMBC)*, Jul. 2020, pp. 3302–3305.
[19] J. Cheng, F. Wei, C. Li, Y. Liu, A. Liu, and X. Chen, "Position-independent gesture recognition using sEMG signals via canonical correlation analysis," *Comput. Biol. Med.*, vol. 103, pp. 44–54, Dec. 2018.
[20] D. Wu, J. Yang, and M. Sawan, "Transfer learning on electromyography (EMG) tasks: Approaches and beyond," *IEEE Trans. Neural Syst. Rehabil. Eng.*, vol. 31, pp. 3015–3034, 2023.
[21] F. S. Botros, A. Phinyomark, and E. J. Scheme, "Day-to-day stability of wrist EMG for wearable-based hand gesture recognition," *IEEE Access*, vol. 10, pp. 125942–125954, 2022.
[22] H. Le, G. M. Spinks, M. I. H. Panhuis, and G. Alici, "Cross-day myoelectric gesture recognition with hybrid multistream CNN-bidirectional LSTM," in *Proc. IEEE Int. Conf. Mechatronics (ICM)*, Feb. 2025, pp. 1–6.
[23] E. Donati, S. Benatti, E. Ceolini, and G. Indiveri, "Long-term stable electromyography classification using canonical correlation analysis," in *Proc. 11th Int. IEEE/EMBS Conf. Neural Eng. (NER)*, Apr. 2023, pp. 1–4.
[24] X. Jiang et al., "Optimizing the cross-day performance of electromyogram biometric decoder," *IEEE Internet Things J.*, vol. 10, no. 5, pp. 4388–4402, Mar. 2023.
[25] X. Jiang et al., "Optimization of HD-sEMG-based cross-day hand gesture classification by optimal feature extraction and data augmentation," *IEEE Trans. Hum.-Mach. Syst.*, vol. 52, no. 6, pp. 1281–1291, Dec. 2022.
[26] H. Shi, X. Jiang, C. Dai, and W. Chen, "EMG-based multi-user hand gesture classification via unsupervised transfer learning using unknown calibration gestures," *IEEE Trans. Neural Syst. Rehabil. Eng.*, vol. 32, pp. 1119–1131, 2024.
[27] D. D. Domenico et al., "Long-term upper-limb prosthesis myocontrol via high-density sEMG and incremental learning," *IEEE Robot. Autom. Lett.*, vol. 9, no. 11, pp. 9938–9945, Nov. 2024.
[28] X. Jiang, C. Ma, and K. Nazarpour, "Plug-and-play myoelectric control via a self-calibrating random forest common model," *J. Neural Eng.*, vol. 22, no. 1, Feb. 2025, Art. no. 016029.
[29] M. R. Islam, D. Massicotte, P. Massicotte, and W.-P. Zhu, "Surface EMG-based intersession/intersubject gesture recognition by leveraging lightweight all-ConvNet and transfer learning," *IEEE Trans. Instrum. Meas.*, vol. 73, pp. 1–16, 2024.
[30] M. E. Benalcazar, L. Barona, L. Valdivieso, X. Aguas, and J. Zea, "EMG-EPN-612 dataset (2.1)," Zenodo, 2020, doi: 10.5281/zenodo.4421500.
[31] E. Eddy, E. Campbell, S. Bateman, and E. Scheme, "Big data in myoelectric control: Large multi-user models enable robust zero-shot EMG-based discrete gesture recognition," *Frontiers Bioeng. Biotechnol.*, vol. 12, Sep. 2024, Art. no. 1463377.
[32] H. Wu, M. Dyson, and K. Nazarpour, "Arduino-based embedded system for myoelectric hand prostheses," in *Proc. 27th IEEE Int. Conf. Electron., Circuits Syst. (ICECS)*, Nov. 2020, pp. 1–4.
[33] H. Wu, M. Dyson, and K. Nazarpour, "Real-time myoelectric control with an Arduino," in *Proc. 27th IEEE Int. Conf. Electron., Circuits Syst. (ICECS)*, Nov. 2020, pp. 1–2.
[34] M. Jabbari, H. Wu, and K. Nazarpour, "Real-time implementation of spatial convolutional network to control myoelectric prostheses," in *Proc. IEEE Int. Instrum. Meas. Technol. Conf. (I2MTC)*, May 2024, pp. 1–6.
[35] N. Zheng, Y. Li, W. Zhang, and M. Du, "User-independent EMG gesture recognition method based on adaptive learning," *Frontiers Neurosci.*, vol. 16, Mar. 2022, Art. no. 847180.
[36] S. Pizzolato, L. Tagliapietra, M. Cognolato, M. Reggiani, H. Müller, and M. Atzori, "Comparison of six electromyography acquisition setups on hand movement classification tasks," *PLoS ONE*, vol. 12, no. 10, Oct. 2017, Art. no. e0186132.
[37] R. N. Khushaba, "Correlation analysis of electromyogram signals for multiuser myoelectric interfaces," *IEEE Trans. Neural Syst. Rehabil. Eng.*, vol. 22, no. 4, pp. 745–755, Jul. 2014.
[38] H. Hotelling, "Relations between two sets of variates," in *Breakthroughs in Statistics: Methodology and Distribution*. Cham, Switzerland: Springer, 1992, pp. 162–190.
[39] A. Gloaguen et al., "Multiway generalized canonical correlation analysis," *Biostatistics*, vol. 23, no. 1, pp. 240–256, Jan. 2022.
[40] B. Vinograde, "Canonical positive definite matrices under internal linear transformations," *Proc. Amer. Math. Soc.*, vol. 1, no. 2, pp. 159–161, Apr. 1950.
[41] P. Horst, "Relations among m sets of measures," *Psychometrika*, vol. 26, no. 2, pp. 129–149, Jun. 1961.
[42] L. C. Parra, "Multi-set canonical correlation analysis simply explained," 2018, *arXiv:1802.03759*.
[43] E. Campbell, A. Phinyomark, and E. Scheme, "Deep cross-user models reduce the training burden in myoelectric control," *Frontiers Neurosci.*, vol. 15, May 2021, Art. no. 657958.
[44] R. Yang et al., "Visual feedback of pattern separability improves myoelectric decoding performance of upper limb prostheses," 2025, *arXiv:2505.09819*.
[45] T. Overton, Z. Al-Mashhadani, S. Y. Raza, J. Whitson, and M. Rakhshan, "Limb position effect in myoelectric control: Strategies for optimisation and standardisation," *BioRxiv*, 2025, doi: 10.1101/2025.09.01.673545.
[46] LIMB-UCF. (2025). *CAPSAS Documentation*. Accessed: Aug. 18, 2025. [Online]. Available: https://github.com/LIMB-UCF/CAPSAS_Documentation
[47] Lab Streaming Layer. (2025). *Lab Streaming Layer (LSL)*. Accessed: Apr. 7, 2025. [Online]. Available: https://labstreaminglayer.org/
[48] K. Englehart and B. Hudgins, "A robust, real-time control scheme for multifunction myoelectric control," *IEEE Trans. Biomed. Eng.*, vol. 50, no. 7, pp. 848–854, Jul. 2003.
[49] H. Wu and K. Nazarpour, "A TinyML-based system for prosthetic control," in *Proc. IEEE 11th Int. Conf. Inf., Commun. Netw. (ICICN)*, Aug. 2023, pp. 549–553.
[50] A. Phinyomark, R. N. Khushaba, and E. Scheme, "Feature extraction and selection for myoelectric control based on wearable EMG sensors," *Sensors*, vol. 18, no. 5, p. 1615, May 2018.
[51] C. Ma and K. Nazarpour, "DistaNet: Grasp-specific distance biofeedback promotes the retention of myoelectric skills," *J. Neural Eng.*, vol. 21, no. 3, Jun. 2024, Art. no. 036037.
[52] A. de Cheveigné et al., "Multiway canonical correlation analysis of brain data," *NeuroImage*, vol. 186, pp. 728–740, Feb. 2019.
[53] X. Wang, D. Ao, and L. Li, "Robust myoelectric pattern recognition methods for reducing users' calibration burden: Challenges and future," *Frontiers Bioeng. Biotechnol.*, vol. 12, Jan. 2024, Art. no. 1329209.
[54] W. Li, X. Zhang, P. Shi, S. Li, P. Li, and H. Yu, "Across sessions and subjects domain adaptation for building robust myoelectric interface," *IEEE Trans. Neural Syst. Rehabil. Eng.*, vol. 32, pp. 2005–2015, 2024.
[55] J. Mencel et al., "Motor imagery training of reaching-to-grasp movement supplemented by a virtual environment in an individual with congenital bilateral transverse upper-limb deficiency," *Frontiers Psychol.*, vol. 12, Mar. 2021, Art. no. 638780.
[56] K. Østlie, R. J. Franklin, O. H. Skjeldal, A. Skrondal, and P. Magnus, "Assessing physical function in adult acquired major upper-limb amputees by combining the disabilities of the arm, shoulder and hand (dash) outcome questionnaire and clinical examination," *Arch. Phys. Med. Rehabil.*, vol. 92, no. 10, pp. 1636–1645, 2011.
[57] A. Radmand, E. Scheme, and K. Englehart, "On the suitability of integrating accelerometry data with electromyography signals for resolving the effect of changes in limb position during dynamic limb movement," *JPO J. Prosthetics Orthotics*, vol. 26, no. 4, pp. 185–193, 2014.
[58] H.-M. Hsu, Y.-C. Lin, W.-J. Lin, C.-J. Lin, Y.-L. Chao, and L.-C. Kuo, "Quantification of handwriting performance: Development of a force acquisition pen for measuring hand-grip and pen tip forces," *Measurement*, vol. 46, no. 1, pp. 506–513, Jan. 2013.
[59] M. Safaie et al., "Preserved neural dynamics across animals performing similar behaviour," *Nature*, vol. 623, no. 7988, pp. 765–771, Nov. 2023.
[60] M. Dabagia, K. P. Kording, and E. L. Dyer, "Aligning latent representations of neural activity," *Nature Biomed. Eng.*, vol. 7, no. 4, pp. 337–343, Nov. 2022.